AIP | Review of Scientific Instruments

Regenerative feedback resonant circuit to detect transient changes in electromagnetic properties of semi-insulating materials

A. Mark Jones, James F. Kelly, Ronald H. Severtsen, and John S. McCloy

Citation: Rev. Sci. Instrum. **84**, 084703 (2013); doi: 10.1063/1.4817537
View online: http://dx.doi.org/10.1063/1.4817537
View Table of Contents: http://rsi.aip.org/resource/1/RSINAK/v84/i8
Published by the AIP Publishing LLC.

Additional information on Rev. Sci. Instrum.

Journal Homepage: http://rsi.aip.org
Journal Information: http://rsi.aip.org/about/about_the_journal
Top downloads: http://rsi.aip.org/features/most_downloaded
Information for Authors: http://rsi.aip.org/authors

ADVERTISEMENT

Regenerative feedback resonant circuit to detect transient changes in electromagnetic properties of semi-insulating materials

A. Mark Jones, James F. Kelly, Ronald H. Severtsen, and John S. McCloy[a)]
Pacific Northwest National Laboratory, Richland, Washington 99352, USA

(Received 7 February 2013; accepted 17 July 2013; published online 8 August 2013)

A prototype regenerative feedback resonant circuit has been developed for measuring the transient spectral response due to perturbations in properties of various electromagnetic materials. The circuit can accommodate a variety of cavity resonators, shown here in the 8 GHz range, with passive quality factors (Q_{stat}) as high as 7000 depending upon material loading. The positive feedback enhanced dynamic quality factors (Q_{dyn}) of resonator/material combinations in the regenerative circuit are on the order of 10^7-10^8. The theory, design, and implementation of the circuit is discussed along with real-time monitored example measurements of effects due to photon-induced charge carriers in high-resistivity silicon wafers and magnetic-field induced perturbations of yttrium-iron garnet. © *2013 AIP Publishing LLC*. [http://dx.doi.org/10.1063/1.4817537]

I. INTRODUCTION

Resonant circuits have long been used to amplify small signals and can be effectively designed directly as environmental sensors. Monitoring of transient changes such as the change in free carrier population in a semiconductor due to electromagnetic radiation absorption is a possible first-order physical change that can be enhanced by resonant circuits. Free carriers can conceivably induce other subsequent electromagnetic (EM) property changes: (1) a change in electrical conductivity (a form of dielectric loss), (2) a change in dielectric permittivity as the free carriers couple with electric dipoles, or (3) changes in magnetic permeability as the free carriers couple with electron spins in magnetic dipoles. Sensor constructs taking advantage of resonator amplification have been proposed for various applications. For example, a chemical sensing platform has been suggested where a reference detection dipole changes its resonant frequency when in the presence of the target chemical, which can then be detected by radar reflectivity.[1] Similar designs have been suggested for radiation detectors using a resonant tank circuit with a semiconductor resistor that changes its electrical properties in response to irradiation, thus generating a frequency shift.[2] Recently, Cetinoneri *et al*. have shown room temperature detection of gamma radiation through power reflection measurements in a microwave cavity containing Cd-Zn-Te in which increased conduction results in change of material conductivity and cavity quality factor due to the electrons created by the ionizing radiation.[3] In that work low noise contactless measurements of the cavity perturbations could be performed in several microseconds using reflected power changes. However, these measurements required a large number of components which may be expensive.

Low phase noise contactless measurements of cavity perturbations can also be accomplished with active (positive) feedback resonant circuits using a regenerative amplifier topology or regenerative oscillator.[4] When the output of an amplified resonator is recombined with proper phase (modulo 2π) into the resonator, the system can sensitively amplify cavity perturbations. This approach can maintain the residual phase noise of the amplifier at a reasonable level while offering a significant Q-factor improvement that can be used to enhance observation of any cavity perturbations over the noise introduced by the amplifier chain.[5] Regenerative amplification (open loop gain < 1) or regenerative oscillation (open loop gain > 1) can provide a very fast response for observing resonant cavity perturbations with a minimum number of required components and was thus pursued in this work. The regenerative oscillator initially conceived by Armstrong[6,7] makes for a low cost, efficient measurement system using reinforcement of the oscillation conditions between the input and output of a low parallel resistance LCR tank resonator.

The fast response time and continuous monitoring provided by the resonant feedback loop is well-suited for studying transient phenomena. Depending upon the circuit implementation and miniaturization, the response time for tracking the resonant frequency changes is estimated to be on the order of 10 to 100 ns (the time for several round-trip feedback cycles of signal buildup); for the prototype circuits described in this work it may be of the order of 30 ns. This cycle time for signal buildup above thermal noise could be greatly improved with miniaturization using RF integrated circuits. This expediency of rapid signal buildup is a hallmark of super-regenerative receivers that are now used in very low power sensor networks.[8] This allows for precise measurements of fast changes in electromagnetic properties that may occur due to various environmental effects interacting with a material inserted into the resonator, since changes in the material properties of the resonator will produce a corresponding change in the signal frequency in the feedback loop. Amplifying the signal directly within the resonant cavity reduces external noise sources and provides the highest signal-to-noise ratio for material change detection. A sudden increase in the noise level

[a)] Author to whom correspondence should be addressed. Current affiliation: Washington State University, School of Mechanical & Materials Engineering, Pullman, WA; john.mccloy@wsu.edu

 © 2013 AIP Publishing LLC

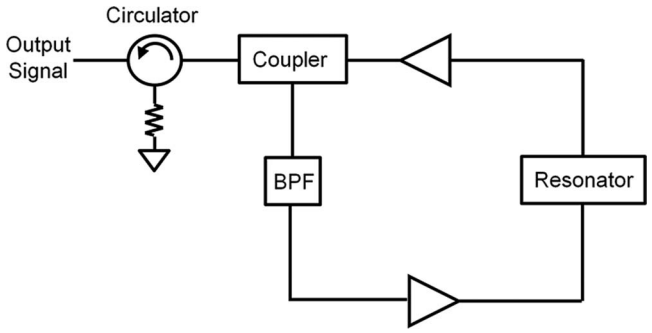

FIG. 1. Block diagram of regenerative feedback resonant circuit used to monitor transient changes in material properties. Amplifiers have their usual symbol, and BPF denotes "band pass filter." Upper amplifier is a low noise (LNA) amplifier, while the lower feedback amplifier is a cascade power amplifier stage with excellent isolation.

near the resonant frequency can also be used to detect transient effects.

In this work, we focus on the development of a highly sensitive resonant circuit that can detect transient changes in the properties of various classes of electromagnetic materials. Section II discusses the fundamental operation of a regenerative feedback resonant circuit, and then describes its implementation as a laboratory prototype sensor for environmental perturbations. Subsequently in Section III, example results are presented using visible light impinging on a high-resistivity silicon wafer and magnetic fields interacting with the soft magnetic material yttrium iron garnet. Section IV then discusses these results in the context of sensor development.

II. MATERIALS AND METHODS

A. Regenerative circuit design

A block diagram of the regenerative circuit developed for transient perturbation experiments is shown in Figure 1, with a photograph of the system shown in Figure 2. The resonant cavity (here called the resonator), which contains the material under test, is located in the feedback loop of several microwave amplification stages. The circuit configuration can be adapted to accommodate essentially any two-port resonant cavity in order to investigate numerous types of possible transducer materials, including magnetic and dielectric materials. If required, a bandpass filter may be placed in the feedback loop to suppress spurious resonances of the resonator. A directional coupler is used to pass the resulting signal through an optional microwave circulator for direct monitoring of the transient behavior or conversion to a lower frequency by another circuit.

Direct evaluation of the output signal transient behavior can be performed using a real-time spectrum analyzer (RTSA). Our work employs a Fourier-based digital spectrum analyzer to perform precision signal analysis, but existing methods of self-referenced signal comparisons could also be used to accomplish sensitive fine-scale analysis of the frequency-phase effects induced by external perturbations.[9–12] The operating frequency of the resonators currently used in the prototype circuit is near 8 GHz. The output signal could be down-converted to a much lower frequency to allow the use of a lower-bandwidth monitoring instrument such as a deep-memory digital oscilloscope.

The circuit was implemented using discrete components with coaxial microwave connectors to maximize design flexibility and reduce the cost of the proof-of-concept prototype. The functional regenerative oscillator circuit shown in Figure 1 was tested with two different commercial resonators on separate aluminum plates (see Figure 2). One resonator was designed to investigate RF polarization (capacitance) changes of wafer materials, while the second resonator was designed to study magnetic permeability changes of cylindrical samples of magnetic ceramics. The fixed components of the regenerative feedback circuit for these 8 GHz resonators are two 0.1–10 GHz wideband power amplifiers[13] in cascade with a 6–18 GHz low noise amplifier,[14] a 7.85–8.95 GHz bandpass filter,[15] a 7–12.4 GHz directional coupler,[16] and a 6–12 GHz circulator.[17]

B. Resonators

Custom microwave resonators were acquired for use in material electromagnetic property characterization studies.[18] These resonators employed a deliberately weak probe and output coupling as they were used in the feedback loop of the regenerative circuit. The operating principles of these cavity resonators are well understood and information on their use can be found in various references.[8,14–18]

Two resonators were used for this work which operated near 8 GHz. The first resonator is a $TE_{01\delta}$ mode split-post

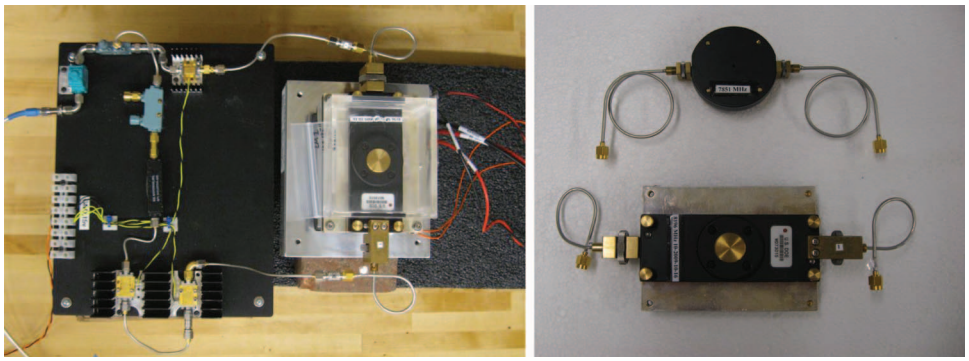

FIG. 2. (Left) Layout of regenerative feedback resonant circuit with 8.2 GHz split-post dielectric resonator mounted on a thermo-electric cooling system. (Right) Commercial resonant cavities (QWED) used in the circuit: (top) 7.85 GHz dielectric ring resonator and (bottom) 8.2 GHz split-post dielectric resonator.

dielectric resonator (SPDR) which operates at 8.2 GHz. It can be used with uniform sheets of dielectric or magnetic material, thin ferroelectric films on a dielectric substrate, and high-resistivity semiconductors.[19,20] The maximum thickness of wafer samples is 1 mm and minimum chord size of the sample is 22 mm. The second resonator is a H_{011} mode dielectric ring resonator (DRR) which operates at 7.85 GHz. It can be used with narrow cylindrical samples of magnetic material which have a maximum diameter of 2 mm.[21,22]

1. Static quality factor measurements (Q_{stat})

In addition to the real-time spectrum analyzer transient measurements performed with the resonators in the regenerative feedback circuit, the resonators may be used without the circuit to accurately characterize the material electromagnetic properties (complex permittivity and complex permeability) from the S-parameters before and after perturbation to determine if permanent changes have occurred.

The static quality factor Q_{stat} of the empty SPDR and DRR cavities was measured using a vector network analyzer (VNA)[23] and the values are shown in Table I. The static quality factor is calculated from a two-port transmission measurement (S_{21}) using a VNA and is defined as

$$Q_{\text{stat}} = f_{\text{stat}}/\Delta f_{-3\text{dB}}, \tag{1}$$

where f_{stat} is the center frequency and $\Delta f_{-3\text{dB}}$ is the bandwidth between the −3 dB frequencies.[24]

2. Dynamic quality factor measurements (Q_{dyn})

We define the dynamic quality factor Q_{dyn} as the Q-factor measured when the regenerative feedback circuit is in operation. Q_{dyn} is obtained from a weak coupling measurement of the circulating power in the regenerative circuit using the RTSA as

$$Q_{\text{dyn}} = f_{\text{dyn}}/\Delta f_{-3\text{dB}}, \tag{2}$$

where f_{dyn} is the center frequency and $\Delta f_{-3\text{dB}}$ is the bandwidth between the −3 dB frequencies.

The Q_{dyn} was obtained by measuring the coupled signal in the feedback loop using the RTSA for the empty resonator in the feedback path of the circuit. The resulting amplification of the static Q-factor by the dynamic feedback technique represents an increase in the frequency selectivity ($Q_{\text{dyn}}/Q_{\text{stat}}$) of a factor of $\sim 10^5$. Values for the Q-factors are shown in Table I.

TABLE I. Measured frequency and Q-factor values for static and dynamic resonator/material configurations.

Resonator	Material	f_{stat} (GHz)	f_{dyn} (GHz)	Q_{stat}	Q_{dyn}	Q-multiplication
SPDR	Empty	8.196	8.193	6694	51 000 000	7.62×10^3
SPDR	Si	8.012	8.034	2599	9 000 000	3.46×10^3
DRR	Empty	7.852	7.859	5234	68 000 000	1.30×10^4
DRR	YIG	7.932	8.521	4081	15 000 000	3.68×10^3

C. Temperature control

The resonator body was mounted onto a thermo-electric cooler (TEC) in order to control the thermal environment of the material under test and thus minimize frequency drift due to temperature changes. A cold plate cooler[25] was used with a proportional–integral–derivative (PID) controller.[26] The TEC system includes a finned heat sink attached to the hot side and a cold plate attached to the cold side of the thermo-electric modules. Aluminum interface plates were designed to provide a path of low thermal resistance between the SPDR and the DRR fixtures and the cold plate. A thermistor was mounted to the side of the cold plate with thermal compound to provide temperature feedback to the controller unit, and a small fan was used to convectively cool the heat sink.

It was found that the temperature of the cold plate could be maintained at 19 °C within 0.1 °C using the TEC system. Only the proportional and integral coefficients of the PID controller were used. The cooling fan was mounted on a separate fixture to prevent physical vibrations from disturbing the output of the resonant circuit. In addition, the entire resonator and TEC assembly was acoustically isolated from the laboratory bench using closed-cell, high-density foam. A rectangular Plexiglas® enclosure was designed to fit onto the resonator platform to protect the material sample from air currents.

D. Transducer materials

Two different material types were selected for use in the resonators to examine effects of perturbations on cavity signals. To demonstrate operation for optical stimulation of charge carriers, a high-resistivity (4000–5000 Ω-cm) silicon wafer was first used. The diameter of the wafer is 50 mm and the thickness is 0.28 mm. The SPDR was used with a VNA and material property extraction software to calculate the ~8 GHz dielectric permittivity (ε') of the wafer to be 11.7 and dielectric loss tangent ($\tan\delta = \varepsilon''/\varepsilon'$) to be 0.005 (consistent with published data[27,28]). The VNA was also used to measure the Q_{stat} of the wafer-loaded SPDR to be 2600. The Q_{dyn} measured with the regenerative circuit with the wafer inserted into the SPDR was measured to be 9 million, which represents an increase greater than 10^3. The second material considered is a multi-crystalline sintered ceramic cylinder of the magnetic material yttrium iron garnet ($Y_3Fe_5O_{12}$ or YIG). The vendor-supplied material extraction software was also used to determine the ~8 GHz magnetic permeability to be 0.8078 (μ') and 0.0003 (μ'') for machined YIG cylinders with ~2 mm diameter inserted in the DRR. Repeatability measurements on the resonators with these samples inserted indicated that the SPDR could determine the real ε' and imaginary ε'' components of permittivity, respectively, $\varepsilon' \pm 0.05$ or better and $\varepsilon'' \pm 0.0005$ or better and, the DRR could determine corresponding complex permeability ($\mu' \pm 0.003$ or better and $\mu'' \pm 0.0003$ or better) when using the VNA. This suggests that the higher dynamic Q-factors obtained with the regenerative feedback circuit should allow even more precise determination of the material property changes.

III. RESULTS

A summary of the configurations tested under static conditions (using a VNA) and tested with regenerative feedback circuit (using a RTSA) is shown in Table I. In every case, the dynamic Q-factor is 10^3 to 10^4 higher than the static Q-factor. The static and dynamic Q-factors were determined using the procedures described in Sec. II.

A. Static resonant frequency (f_{stat})

The slight change in resonant frequency of the loaded versus the unloaded resonators, as measured by the VNA, is consistent with the effects of material loading and can be understood as follows. The resonator can be approximated as a tank circuit composed of a lumped inductor, capacitor, and the series sum of their parasitic resistances.[20] The resonant frequency of this circuit can be estimated as

$$\omega_0 = 2\pi f_0 = \frac{1}{\sqrt{LC}}, \tag{3}$$

where ω_0 is the angular frequency in radians/s, f_0 is the frequency in Hz, L is the inductance, and C is the capacitance. In either resonator example without feedback, the circuits are fairly well described by lumped elements of a discrete inductor L and capacitor C, along with a sum of series resistance terms that can be treated as a lumped resistor R. The lumped parameters for the reactive parts of the circuits can be scaled as geometrically equivalent terms, as $L \propto \mu_r\ \mu_0 \pi r^2/l$ and $C \propto \varepsilon_r\, \varepsilon_0\, A/d$, where r, l, A, and d are specific to the geometry. In the case of the SPDR, r and l would describe characteristic dimensions of the split-post inductor's radius and length, respectively, while it would be the characteristic dimensions for the inner annulus of the dielectric ring holding a cylindrical sample in the DRR, and so forth with A and d for the area of the capacitor and its gap separation of each of resonator design. Substituting these values into (3) we obtain a zeroth order equation for resonant frequency of a materially loaded resonator in terms of the material loading parameters:

$$f_0 = \frac{1}{2\pi}\left(\frac{c}{r}\right)\sqrt{\frac{d * l}{\pi * A * K}}, \tag{4}$$

where by definition the speed of light $c = 1/(\varepsilon_0\mu_0)^{-1/2}$ and K, the loading-material dependent constant, is described in terms of its relative dielectric permittivity ε_r and relative magnetic permeability μ_r, as

$$K = \left(\frac{\varepsilon}{\varepsilon_0}\right)\left(\frac{\mu}{\mu_0}\right) = \varepsilon_r \mu_r. \tag{5}$$

Thus, it can be seen that the change of the permittivity (ε_r) or permeability (μ_r) of the material-loaded gap or cylindrical annulus in the resonators directly affects the resonant frequency in a specified way. Though the DRR and SPDR resonators described here are different in detail, the relationship to ε_r and μ_r is the same. An empty resonator of the SPDR type has $\varepsilon_r = 1$ (air), while a dielectric-loaded one has $\varepsilon_r > 1$. This increase in permittivity results in a decrease of resonant frequency, as is observed in this case. An empty resonator of the DRR type has $\mu_r = 1$ (air) while a magnetic-loaded one can have $\mu_r > 1$ or $\mu_r < 1$ depending on the relative position of the gyromagnetic resonance frequency.[21] In this case, the operating frequency of the resonator is higher than the gyromagnetic resonance frequency of the YIG sample and, therefore, $\mu_r < 1$. Thus, the permeability in the circuit decreases, and the resonant frequency of the circuit increases, as is observed.

B. Dynamic resonant frequency (f_{dyn})

The change in the dynamic resonant frequency (f_{dyn}) from the static frequency (f_{stat}) can be understood as follows. The additional phase shift introduced in the resonant loop by components such as amplifiers and transmission lines causes the phase self-locking behavior of the circuit to resonate at a different frequency.[29] The round-trip phase shift at the resonant frequency must be a multiple of 2π radians to satisfy the Barkhausen oscillation condition.[30] Depending on the phase shift, this may result in a stable f_{dyn} of greater or less than f_{stat}. Phase delays introduced by coaxial cables and connectors are compensated by the operational frequency of the amplifier phase margins to assure proper modulo-(2π) phase self-locking behavior of the entire circuit. So the feedback circuit may self-resonate at a frequency different from the static frequency of the loaded resonator as measured with the VNA. It may be coincidental that the empty resonator static frequencies lie very close to the dynamically measured resonant frequencies, or this may be a feature of properly setting up the resonators to prescribed S-parameter conditions of weak feed probe coupling.

C. Static (Q_{stat}) and dynamic (Q_{dyn}) quality factors

Figure 3 shows an illustration of the static signal (measured with a VNA) and the feedback circuit signal (measured with a RTSA) from the SPDR with and without the high resistivity silicon wafer. Figure 3(a) demonstrates the dramatic narrowing of the resonant response due to the regenerative feedback circuit. It also shows that the introduction of the wafer lowers the resonant frequency, as would be expected from an introduction of a higher permittivity substrate in the resonator's air gap. Figures 3(b) and 3(c) show the static resonance of the unloaded and Si-loaded measurements, respectively, indicating the determination of the static Q-factor. Analogously, Figures 3(d) and 3(e) show the dynamic resonance of the unloaded and Si-loaded measurements, respectively, indicating the determination of the dynamic Q-factor. At this point, we have not formulated a generalized analytical relationship between Q_{dyn} and Q_{stat}. It appears that the network analysis in Ref. 5 provides a method for calculating the Q-multiplication factor using the loop gain and the loaded and unloaded Q-factors of the resonator.

D. Transient photo-conductivity measurements using feedback system

The change in the output signal of the regenerative feedback circuit containing the SPDR and silicon wafer was measured using the digital phosphor spectrum display of a RTSA. This displays transient signals in such a way that a color scale

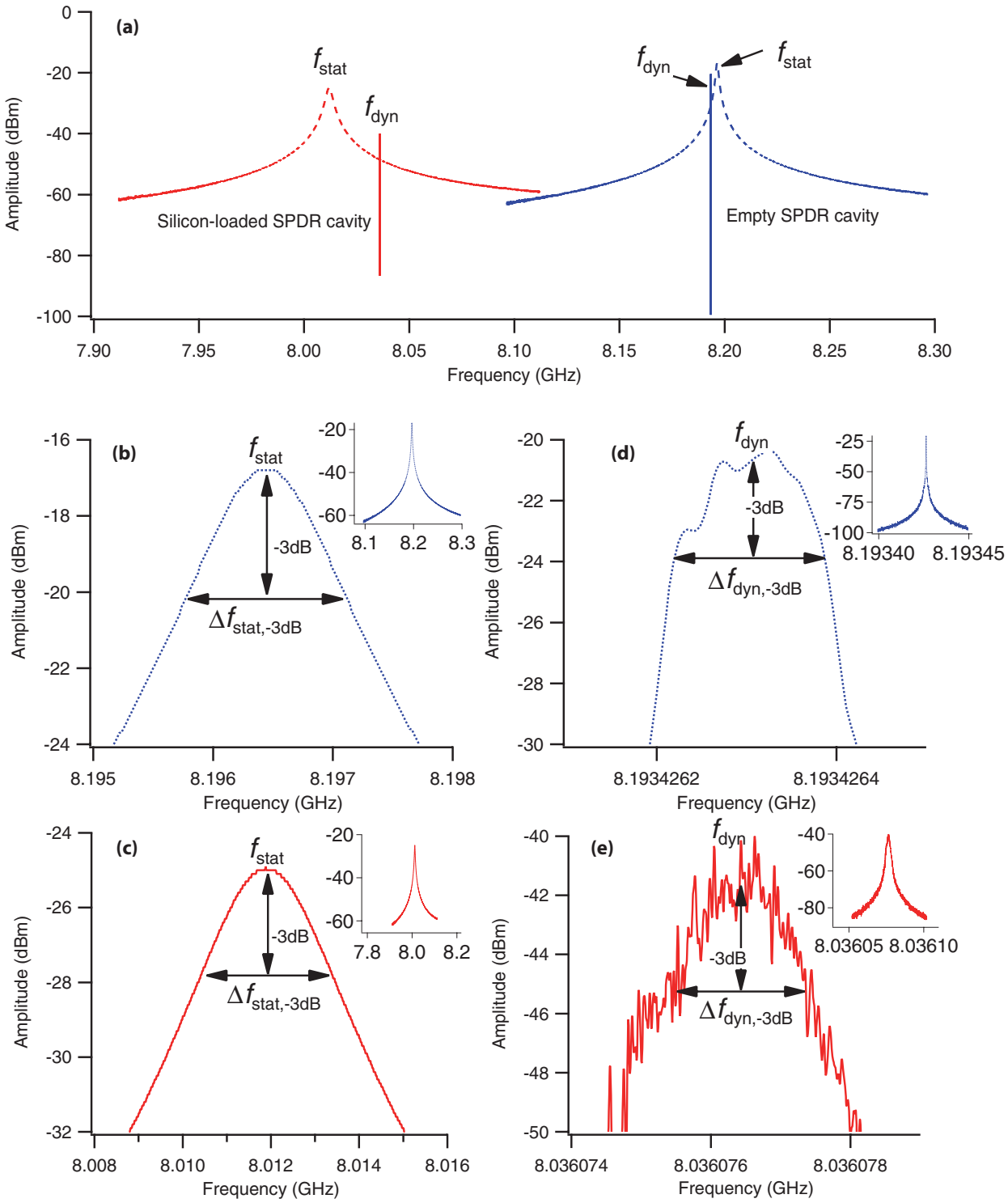

FIG. 3. Illustrations of the sharpening of the resonance that happens as a result of introducing feedback and frequency shift due to material introduction. (a) Comparison of static (VNA) and dynamic (RTSA) resonances for empty and Si-loaded SPDR; (b) VNA signal for unloaded SPDR; (c) VNA signal for Si-loaded SPDR; (d) RTSA average of 10 sweeps for unloaded SPDR; (e) RTSA average of 10 sweeps for Si-loaded SPDR. Insets in (b) through (e) show the full signal (same axes designations as the main figure) while the main portion of each shows a closeup used in determining the Q-factor.

can represent time passed since the signal was measured.[31] The measurement has 110 MHz of real-time acquisition bandwidth and can display 292 000 spectrum updates per second to capture transient events with a minimum duration of 5.8 μs. The advantage of this instrument over a traditional swept spectrum analyzer is the ability to seamlessly capture a signal in real time for frequency spans up to 110 MHz.[32] This is enabled by the use of a RF down-converter and wideband intermediate frequency (IF) signal that is digitally sampled at a rate that exceeds the Nyquist sampling theorem by ~50%

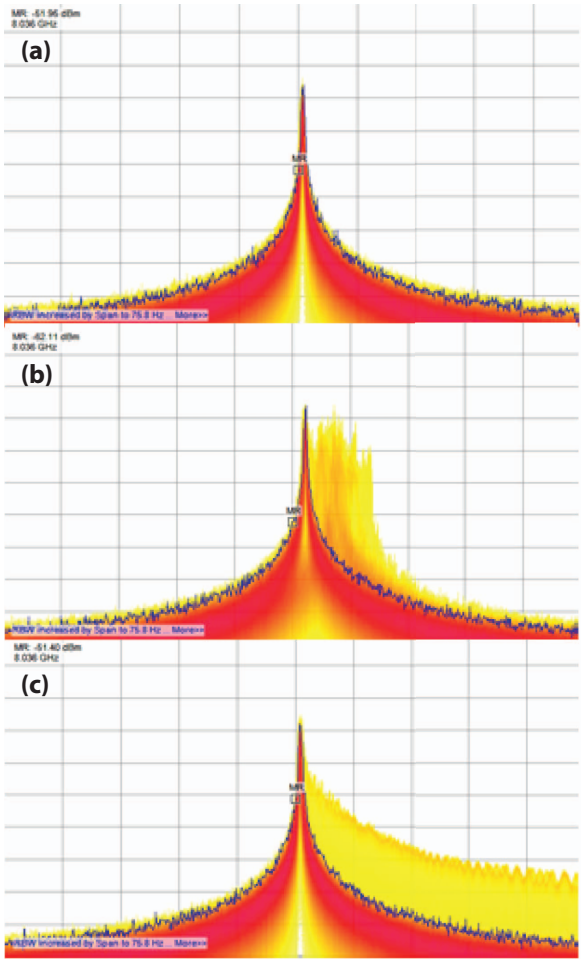

FIG. 4. Digital phosphor spectrum display of regenerative feedback circuit response with silicon wafer inserted into SPDR. (a) Before perturbation; (b) illuminated with red laser pointer; (c) illuminated with Xe camera flashbulb. Note that the frequency content of the flashbulb response continues out to higher frequencies than is shown in this figure.

(specifically, 375 MSamples/s). The persistence of each pixel in the bitmapped spectrum display was set to 5 s in order to easily view changes in the signal behavior. The pixels of the digital phosphor display are also color-coded based on the frequency of occurrence.

Figure 4(a) shows a frame capture of the digital phosphor spectrum display for the baseline condition with the silicon wafer and SPDR in the feedback path, where the frequency span was set to 500 kHz and vertical axis was set to 10 dB/division. Figure 4(b) shows a frame capture taken while a red laser beam from a handheld laser pointer was used to illuminate the wafer. The pixel activity on the upper side of the resonant frequency indicates the rapid transient changes in the frequency response produced by a mechanically modulated laser source. In this case, the frequency changes were on the order of +50 kHz depending upon where the laser beam illuminated the high resistivity silicon wafer. The transient behavior in the signal due to the charge carrier generation and recombination can easily be displayed and studied using the digital phosphor display with the pixel persistence feature. Figure 4(c) shows a frame capture of the spectrum display taken while a xenon flashbulb from a handheld digital camera was used to illuminate the silicon wafer. In this case, the transient disturbance is distributed over a wider frequency range on the upper side of the resonant frequency. Experiments showed that the bandwidth of the disturbance was dependent upon the intensity of the incident light (i.e., the distance between the flashbulb and the edge of the silicon wafer).

In addition, it was determined that the circuit resonance could be shifted by approximately −20 kHz by turning off the overhead fluorescent lights in the laboratory. This series of experiments with optical stimulation of charge carriers in a semiconductor material demonstrate the ability of the regenerative circuit to detect short duration transient events. It should be noted that each of these photon interaction events shows a characteristic frequency response that can be readily distinguished.

The qualitative behavior of the SPDR with silicon loading in response to different kinds of light can be understood as follows. Charge carriers in a semiconductor are photoexcited across the energy bandgap to create absorption. The change in the absorption spectrum results in a change in the refractive index through the Kramers-Kronig relation of coupled optical constants.[33] The absorption is related to the imaginary component of the dielectric permittivity (ε''), depends on the relative importance of processes such as one-photon absorption (interband transition) and free-carrier absorption (phonon-assisted intraband transitions and intervalence-band transitions), and also varies with carrier concentration.[33] Other effects, such as relative importance of bandfilling and bandgap shrinkage, determine the blue or red-shift of the absorption edge.[34,35] This absorption, induced by optical or electric carrier injection,[34] then results in refractive index (or real permittivity) change that is a function of frequency. At low energies, such as in the microwave region, and at sufficient enough carrier densities, the change in real permittivity is negative.[33,34,36] The absolute change in ε' and ε'' is a function of carrier mobility as well.[36]

Measurements of microwave photoconductive decay are now being developed as a sensitive measure of the photo-induced carrier lifetimes.[37–40] The need is to understand, nondestructively and using noncontact techniques, the quasi-steady-state photoconductance of nascent Si wafers and/or surface passivated for optoelectronic and photovoltaic devices, such as high efficiency solar cells. The measurements in Ref. 38 are similar in scope to this work, but use a balanced two-beam microwave transmission interferometer at 9.35 GHz to observe effects of focused laser light on unprepared clean silicon wafers. That work uses fairly high incident power from a fiber laser at 532 nm to introduce light to the wafer edges of silicon samples with resistivities up to 1000 $\Omega \cdot$cm, as well as adjustable excitation fluence up to 3.3 mW/cm^2. It was found that the free carrier optical absorption effects of these microwave absorption-transmission studies were well explained by the Drude model of photoconductance. Essentially, free carriers will vibrate strongly in the applied electrical field of a microwave system operated at a few cm wavelength, causing large changes of the substrate's net polarization. The real and imaginary components of the microwave permittivity ε' and ε'' with free carriers from

photoabsorption are typically given as

$$\varepsilon' = \varepsilon_r/\varepsilon_0 = n^2 - k^2 = \varepsilon_{\mathrm{Si}}(1 - [\omega_P\tau]^2/\left(1 + [\omega_P\tau]^2\right), \tag{6}$$

$$\varepsilon'' = \varepsilon_i/\varepsilon_0 = 2nk = \varepsilon_{\mathrm{Si}}([\omega_P\tau]^2/(1 + [\omega_P\tau]^2)), \tag{7}$$

where ω_{P} is the plasma angular frequency of the semiconducting silicon, $\varepsilon_{\mathrm{Si}}$ is the real part of the dielectric constant of intrinsic silicon due to tightly bound valence electrons, n is the real part of the microwave index of refraction, k is the microwave extinction coefficient induced by free carriers via optical absorption, and τ is the lifetime of the photo-induced charge carriers. As noted in Ref. 38, ε' will decrease when additional charge carriers are created by optical absorption. The effect on the extinction coefficient k is quite large at microwave frequencies below the plasma frequency. The resultant transient polarization change on ε' (diminished by k^2) is expected to be fairly large at microwave frequencies near 8 to 10 GHz.

A reduction in ε', combined with an increase in ε'', should result in a shift of the regenerative feedback resonator signal to a higher frequency and a reduction in the Q-factor. This is, in fact, what is observed in Figures 4(b) and 4(c), in that the signal of the photoexcited resonator shifts to the right (higher frequency) and its intensity is dampened (lowered Q). Consistent with this observation, the dynamic feedback resonance frequency shifted to lower frequencies when the ambient fluorescent lights were turned off. The permittivity change as determined from the resonator measurements could thus, in principal, be converted into absorption and then into free carrier measurements or conductivity.[36] Related measurements include transient microwave absorption determination of conductivity and carrier lifetimes using pulse-probe techniques, where the probe is a microwave beam.[41–43] The advanced method of transient microwave photoconductivity is even more similar, being based on the insertion of a semiconductor or dielectric into a cavity and simultaneously determining the frequency shift (photo-dielectric effect, due to trapped electrons) and the Q-factor change (photoconductive effect, due to free electrons).[36]

The spectral content of the resonator signature from the flash bulb (typical xenon arc lamp from a commercial camera) provides additional evidence of the utility of the RTSA technique. For comparison, non-destructive lifetime measurements of the excess carrier photocharges by microwave reflection changes have used fairly powerful optical xenon flash lamps ($\bar{\lambda} \sim 550$ nm) with incident fluence of 30 W/cm^2 and $\sim$3 μs durations to effect a transient microwave reflection.[44] Discharge durations for typical photographic xenon flashtubes such as those used in this work range from 1 μm to 10s of milliseconds, but do not have the high fluences compared to the noted work of Borrego.[44] Since the update rate for the RTSA is $\sim$5.8 μs, it is likely that the observed very large increase in resonant frequency offsets with concomitant Q-spoiling is due to the impulse of visible radiation of the xenon. What is compelling about this work is that the flashlamp spectrum is in the blue end of the visible where the optical absorption coefficient for intrinsic silicon is quite large (absorbance [cm^{-1}] $\sim$ [1 to $<$ 10 μm]$^{-1}$) meaning that the signals shown in Figure 4(c) are actually from fairly shallow penetrations into the wafer from weak light scattered into the gap of the SPDR resonator. That the transient signal is quite strong is surprising compared to the results of Borrego.[44] Tests with a time-modulated monochromatic near-IR diode laser with $\lambda > \sim 0.95$ μm should allow us to probe more deeply and uniformly into the wafer and test ultimate sensitivity for bulk volumetric changes.

E. Transient magnetization measurements using feedback system

Similar transient behavior can be observed in the regenerative feedback circuit which uses a DRR and monitors the changes in resonance due to magnetic field perturbations. The effect of saturating a soft magnetic material which is loaded into a DRR operating above the gyromagnetic resonance is to reduce the resonant frequency (see Figure 5(a)). For example, the empty DRR had a static resonant frequency (f_{stat}) of 7.852 GHz, which increased to 7.932 GHz with a YIG sample, and further decreased to 7.833 GHz when a strong permanent magnet was held close to the same YIG sample while in the resonator. Similar results were obtained when magnetizing other soft magnetic samples in the resonator. The downshift in the resonant frequency when magnetized can be explained by the increase in the real part of the magnetic permeability (μ') from 0.8078 in the magnetically unsaturated case to 0.9974 when magnetized. The Q-factor was slightly reduced in the magnetized case, which is likely due to the incomplete saturation of the material and demagnetizing fields on the surfaces of the sample, giving a computed increase of the imaginary component (μ'') from 0.0003 in the demagnetized case to 0.0006 with the permanent magnet. Since the frequency of the DRR is higher than the gyromagnetic resonance frequency of YIG itself (which is $\sim$5 GHz[21]), the losses as represented by μ'' are expected to be small even in the demagnetized case and μ' is expected to be $<$1, as was confirmed. If a magnetic material such as YIG is loaded into a resonator which operates at frequencies below its gyromagnetic frequency (i.e., $<$5 GHz), the Q-factor of a demagnetized sample will be very low due to the "low-field losses" associated with dynamic interaction of oppositely magnetized domains which are present in non-saturated soft magnets.[45,46] In this case, the addition of a feedback resonant circuit can increase the Q-factor to usable levels even without application of an external magnetic field.

The magnetically loaded resonator with regenerative feedback circuit allowed additional observations of the effect of amplification on resonator perturbations. The addition of the feedback loop to the empty DRR resulted in a slight increase in center frequency, from 7.852 GHz in the static measurement to 7.859 GHz in the dynamic measurement (see Figure 5(b)). The frequency increase for the YIG-loaded DRR was much more dramatic, increasing from 7.932 GHz to 8.521 GHz in the feedback circuit. As can be seen in Figure 5(b) and Table I, the Q-factors improved dramatically with inclusion of feedback with the DRR as well. Using the RTSA, we observed the effects of a moving magnetic field near the resonator supplied by a permanent magnet

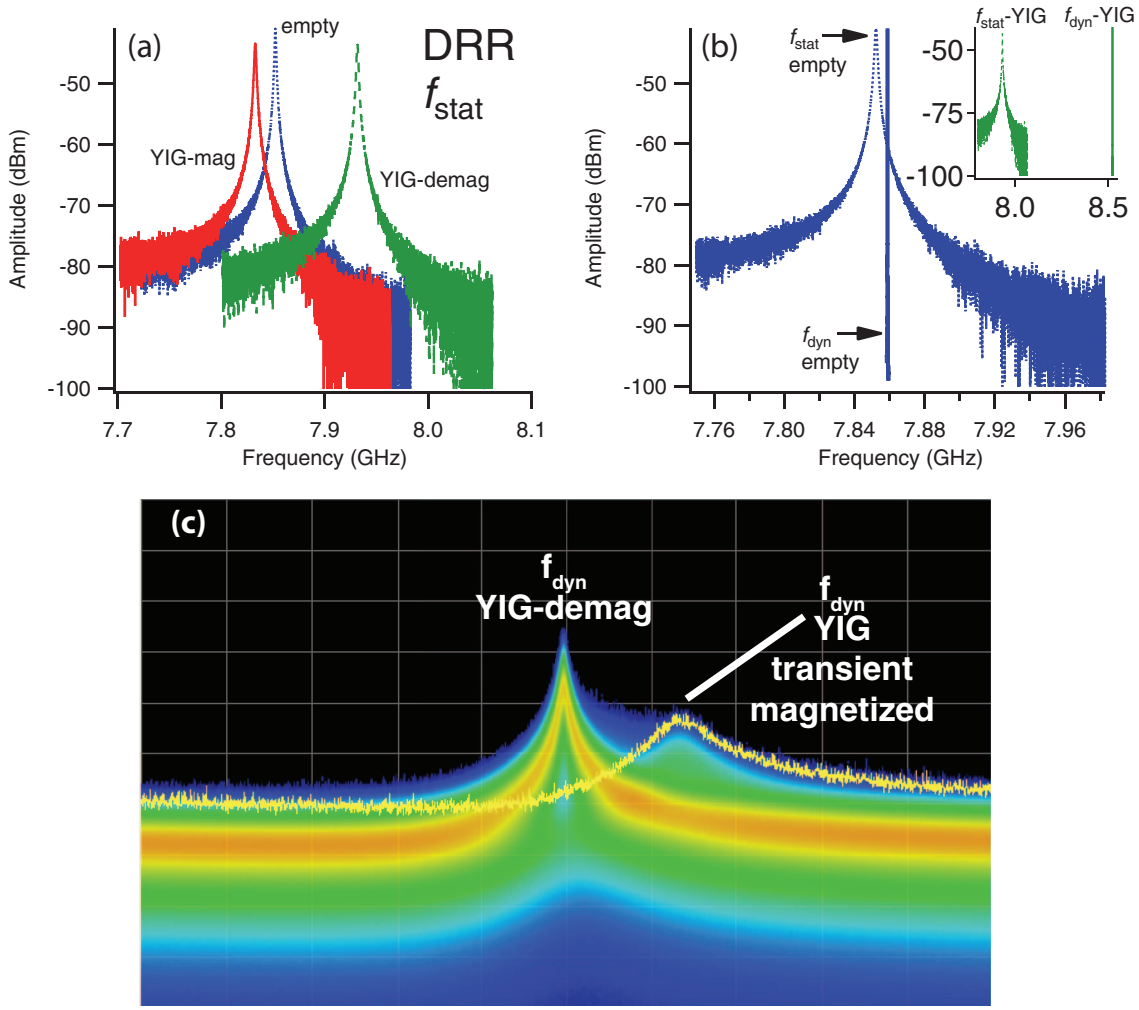

FIG. 5. Resonator experiments with the DRR. (a) Static VNA measurements of empty, YIG-loaded (demagnetized), and YIG-loaded (magnetized); note that a demagnetized YIG-loaded DRR resonates at higher frequency than the empty cavity, but a magnetized YIG-loaded DRR resonates at slightly lower frequency than the empty cavity; (b) static versus dynamic (feedback) measurements for empty (main figure) and demagnetized YIG-loaded (inset) DRR; note the dramatic sharpening of the resonance and slight shift to higher frequency for the empty DRR but large positive frequency shift, resulting in a resonance >8.5 GHz, for the YIG-loaded DRR; (c) RTSA digital phosphor display of a permanent magnet perturbing a YIG-loaded DRR. The center frequency (center of figure) is 8.52146 GHz. It can be seen that interaction with the external magnetic field shifts the feedback resonance to higher frequencies and dampens it.

(Figure 5(c)). The sharp center frequency represents the original resonance of the stable YIG-loaded circuit (~8.521 GHz), while the sideband on the high frequency side represents the effect of the hand magnet on the resonance, broadening and shifting it. We, therefore, see that the same principals for observing transient effects due to opto-electronic effects in the SPDR can be used to observe transient effects due to magnetic fields in the DRR.

IV. DISCUSSION

A. Mechanism of *Q*-factor enhancement

Properly phased positive feedback can increase the overall gain to sustain and reinforce oscillations within a resonant element.[47,48] Positive feedback occurs when the round-trip phase shift of the feedback signal passes through an integer multiple of 2π radians, thus producing regenerative feedback that reinforces the signal strength. The addition of a resonator to the feedback loop serves to filter the signal so that only the frequency band of the resonator is amplified. This type of circuit was patented by Armstrong in 1914 for use as a high-sensitivity radio receiver,[6,7] and this elegant design is still finding applications today.[49] Increases of 10^3 to 10^5 times for signal gain and observed passive quality factor (Q_{stat}) of the circuit (or Q-enhancement of the free standing resonator) are achievable due to positive feedback.[50] In the vicinity of a inductive-capacitive (LC) tank resonance, the resistance in series (R_S) with the inductor, which limit the Q-factor, can be approximated by a parallel conductance (G), resulting in parallel L, C, and G.[49] In this case the conductance $G = 1/[R_S(1 + Q^2)]$, where Q is the static quality factor of the resonator and R_S is parasitic series resistance. The effect of adding positive feedback is to introduce an effective negative conductance term that can compensate for the losses of the net resistance in the circuit which limit Q_{stat} and

increase the dynamic Q-factor (Q_{dyn}). This effect is discussed as a Q-multiplier to enhance received signals in radio systems.[5] Assuming a particular resonant circuit design, Q_{dyn} can be estimated.[49]

B. Regenerative amplification as a general sensor solution

Regeneration amplification is a general technique applicable to many physical systems, and can be used as long as there is a gain stage that can supply energy to a resonant circuit.[47] In addition to studying the capacitive displacement currents in samples, this approach is used with magnetic and optical materials. Q multiplication has been used, for example, to increase signals for nuclear magnetic resonance experiments.[51]

The concept being employed is a variation of active oscillator systems, wherein the material under study is made part of a self-excited or direct feedback-oscillator topology. Unlike transient capacitance measurements,[52,53] such as deep level transient spectroscopy or its optically aided methods of injecting charge into semi-insulators,[37–40,44,54] this approach can investigate the environmental sensitivities of the load material directly with precision frequency-phase analysis. Small deviations of the round-trip loop phase produce observable changes in frequency, which are ascribed to specific environmental perturbations. Corresponding efforts to perfect low phase-frequency noise oscillators, such as quartz oscillators, deliberately strive to understand how to make a feedback based oscillator of high spectral purity.[55]

It is known from this area of work that environmental changes within a resonator structure can be accurately sensed with frequency-phase techniques of radio frequency (RF) electronics. Often this technique makes use of the large Q-factor enhancement of the loaded oscillator to specifically track certain environmental parameters of perturbation. Howe *et al.*[9] describe one such variant to study the spectral purity and perturbations of a direct feedback based oscillator.

C. Regenerative amplifiers in optical applications

The increase in the resonator Q-factor is known in the laser community as gain-narrowing for single pass regenerative amplification.[47] Regenerative laser oscillations result when a suitably large number of round-trips in the laser cavity can be sustained before emission through the partially lossy output cavity mirror.[47,56] Siegman notes that the analysis used with optical regenerative systems could equally apply to analogous mechanical, acoustic, and electrical systems.[47] Regenerative circuits with LC or dielectric resonators in the feedback loop have been used to construct many types of devices, notably low phase noise microwave oscillators.[57,58]

Siegman calculates the regenerative noise amplification in a laser and derives an expression for the classic Schawlow-Townes formula for the dynamic reduction of bandwidth of a regenerative laser oscillator that scales as $1/P(Q_{stat})^2$, where P is the circulating power in the laser cavity. Interestingly, this is the same pre-scaling factor for an LC-feedback oscillator introduced by Leeson to account for its reduced noise spectrum with an ideal active amplifier with negligible phase noise or amplitude noise.[59,60] Howe *et al.*[9] describes accurate correction terms for the feedback amplifier circuit, but also contains a pre-factor of $1/P(Q_{HL})^2$, where Q_{HL} is the half-loaded resonator Q-factor that would give optimal suppression of amplifier and circulator phase noise terms. An optimal coupling to the resonator is suggested in Refs. 9–12 where the input probe (from the output stage of the power amplifier stage) is adjusted to give a high coupling coefficient ($\beta \sim 0.95$), while the output probe to the low noise amplifier stage is kept in a weak coupling limit ($\beta \sim 0.02$). In the work described here we did not attempt this optimization, as both probes were adjusted for weak coupling to avoid distortions by closely spaced higher modes of our commercial resonator, and to preserve the symmetry in the transfer characteristic of the main cavity resonance. As such, our resultant Q-enhancements and potential suppression of amplifier and circulator noise terms are not expected to be optimal for best Q-enhancement or signal recovery of perturbation signals within the loaded resonator.

For the case of regenerative optical amplifiers, the amplification bandwidth can become quite narrow.[47] Practical modes of a laser resonator cavity might have their static bandwidth reduced from ~500 MHz to <500 kHz, yielding a narrow gain-bandwidth product to filter external noise. However, as is the case for early variants of optical feedback cavities, the feedback loop typically has a long time delay, which leads to large phase shifts and resultant large frequency pulling due to environmental vibrations. If the time delay is large there will be rapid, large changes of the phase shift reducing the cumulative gain condition.

Maintaining the necessary precision of the round-trip phase coherence generally makes regenerative amplification excessively delicate to be practical at optical frequencies, but it is quite practical with RF/microwave feedback circuits. As was shown here, using high gain low-noise RF amplifiers and moderately long physical coaxial lines, the regenerative oscillator demonstrated gain narrowing or Q-enhancements exceeding 10^3. It is expected that with much shorter delay times for a round-trip, even higher Q-enhancements may be feasible along with increased gain of any resonant signal change in the feedback resonator.

V. CONCLUSIONS

A laboratory prototype microwave circuit which employs regenerative feedback in a configuration to detect transient changes in material electromagnetic properties has been developed. The circuit exhibits very high selectivity around the resonant frequency with dynamic quality factors as high as 50 million for empty resonators and 15 million under material loading. The dynamic and static quality factors were measured using a RTSA and VNA, respectively. The circuit can be adapted to utilize various types of cavity resonators in order to perform experiments for many dielectric and magnetic materials. The fundamental operation of the device has been verified for dielectric and magnetic samples.

Various optical sources were used to perturb a high-resistivity semiconductor in a split-post dielectric resonator,

demonstrating that transient changes in the circuit response could be effectively captured using a real-time spectrum analyzer. Likewise, a dielectric ring resonator containing an insulating magnetic material demonstrated high sensitivity to a moving permanent magnet. These types of feedback resonator circuits offer very high *Q*-factors for precision materials property measurements and when combined with a real-time spectrum analyzer, a dramatic means of visualizing transient changes in material properties due to external perturbations such as light and magnetic fields.

The work may be most relevant for the rapid and straightforward study of conductivity and ac susceptance changes of materials with very high resistivity, such as semi-insulating (SI) semiconductors. SI semiconductors are becoming an important material class for study leading to advanced microelectronics and optoelectronic materials. A variety of classical techniques have been devised to study the purity of base substrates and the subsequent passivation of these processed materials, in order to improve their efficiencies for energy conversion (solar cells) or electronic switching that typically comes with improved high-resistivity semiconductor materials.

We believe that the power of this technique, especially to understand photoconductive properties of SI semiconductors, is the ability to do contactless analysis of high resistivity materials, without any need to apply Ohmic leads to the samples. The examples shown utilized commercial two-port resonators to study high resistivity silicon and a magnetic ceramic, suggesting a variety of low polished wafers or sintered cylindrical-cut high resistivity materials can be studied.

Because of the high sensitivity and small number of required circuit components, we are also researching this technique to design sensitive environmental sensors. The technique may allow for RF signaling at moderate stand-off ranges to interrogate sensors placed in extreme environments.

ACKNOWLEDGMENTS

This work was supported in part by the Defense Threat Reduction Agency IACRO 11-4485I and in part by Laboratory Directed Research and Development. Pacific Northwest National Laboratory is operated for the U.S. Department of Energy (DOE) by Battelle under Contract NO. DE-AC05-76RL01830. The authors thank Justin Fernandes and Jonathan Tedeschi for their assistance with some of the measurements.

[1]M. G. Bray, A. E. Kovalev, Z. Bayraktar, D. H. Werner, and T. S. Mayer, in *Antennas and Propagation Society International Symposium* (IEEE, 2007), p. 1513.
[2]R. Burger, S. Nuspl, R. Spitzer, E. Wuori, and F. Zieber, U.S. patent 7,220,968 (22 May 2007).
[3]B. Cetinoneri, Y. A. Atesal, R. A. Kroeger, G. Tepper, J. Losee, C. Hicks, M. Rasmussen, and G. M. Rebeiz, in *Microwave Society IMS* (IEEE, 2010), p. 469.
[4]R. Boudot and E. Rubiola, IEEE Trans. Ultrason., Ferroelectr., Freq. Control **59**, 2613 (2012).
[5]C. Novero and G. Brida, *Q-Multiplier: Some Experiments and Few Considerations on Regenerative Circuits* (2002), http://www.inrim.it/~brida/Q_multiplier.htm, Electronic article, accessed July 27, 2011.
[6]E. A. Armstrong, U.S. patent 1,113,149 (6 October 1914).
[7]E. A. Armstrong, Proc. IRE **5**, 145 (1917).
[8]J.-Y. Chen, M. P. Flynn, and J. P. Hayes, in *Proceedings of the IEEE on Custom Integrated Circuits Conference*, San Jose, CA, 21–25 September 2005, p. 361.
[9]D. A. Howe, A. S. Gupta, C. Nelson, and F. L. Walls, U.S. patent 7,075,378 (11 July 2006).
[10]A. S. Gupta, D. A. Howe, C. Nelson, A. Hati, F. L. Walls, and J. F. Nava, IEEE Trans. Ultrason. Ferroelectr. Freq. Control **51**, 1225 (2004).
[11]E. N. Ivanov, M. E. Tobar, and R. A. Woode, IEEE Microw. Guid. Wave Lett. **6**, 312 (1996).
[12]E. N. Ivanov, M. E. Tobar, and R. A. Woode, IEEE Trans. Microwave Theory Tech. **46**, 1537 (1998).
[13]*Wideband Power Amplifier*, AMF-3D-00101000-40-21P (MITEQ®, Hauppauge, NY, USA).
[14]*Low Noise Amplifier*, S4-06001800-20-10A (MITEQ®, Hauppauge, NY, USA).
[15]*Bandpass Filter*, BFV 8400/X1100-0/0 (K&L Microwave, Salisbury, MD, USA).
[16]*Directional Coupler*, 4015C-10 (L-3 Narda Microwave East, Hauppauge, NY, USA).
[17]Circulator, 1090IQ, formerly Innowave now Crane Aerospace & Electronics STC Microwave Systems, Chandler, AZ, USA.
[18]QWED, *The Family of Dielectric Resonators for Precise Measurements of Electromagnetic Properties of Materials at Microwave Frequencies*, http://www.qwed.com.pl/resonators.html.
[19]J. Krupka and J. Mazierska, IEEE Trans. Instrum. Meas. **56**, 1839 (2007).
[20]D. M. Pozar, *Microwave Engineering* (John Wiley & Sons, Hoboken, NJ, 2005).
[21]J. Krupka and R. G. Geyer, IEEE Trans. Magn. **32**, 1924 (1996).
[22]L. F. Chen, C. K. Ong, C. P. Neo, V. V. Varadan, and V. K. Varadan, *Microwave Electronics: Measurement and Materials Characterization* (John Wiley & Sons, 2004).
[23]*Vector Network Analyzer*, PNA E8361A (Agilent, Santa Clara, CA, USA).
[24]J. Baker-Jarvis, M. D. Janezic, B. Riddle, C. L. Holloway, N. G. Paulter, and J. E. Blendell, NIST Technical Note **1520**, 27 (2001).
[25]*Cold Plate Cooler*, CP-031 (TE Technologies, Traverse City, MI, USA).
[26]*PID Controller*, TC-40-20 (TE Technologies, Traverse City, MI, USA).
[27]M. N. Afsar and H. Chi, Int. J. Infrared Millim. Waves **15**, 1181 (1994).
[28]J. Krupka, J. Breeze, A. Centeno, N. Alford, T. Claussen, and L. Jensen, IEEE Trans. Microwave Theory Tech. **54**, 3995 (2006).
[29]N. Yu, E. Salik, and L. Maleki, Opt. Lett. **30**, 1231 (2005).
[30]J. R. Smith, *Modern Communication Circuits* (WCB McGraw-Hill, New York, 1998).
[31]*Real-Time Spectrum Analyzer*, 6114A including options 110 and 200 (Tektronix®, Beaverton, OR, USA).
[32]Tektronix, *Fundamentals of Real-time Spectrum Analysis*, Electronic document, http://www.tek.com/primer/fundamentals-real-time-spectrum-analysis, accessed 7/31/2013.
[33]Z. G. Yu, S. Krishnamurthy, and S. Guha, J. Opt. Soc. Am. B **23**, 2356 (2006).
[34]P. P. Paskov, Solid State Commun. **82**, 739 (1992).
[35]P. P. Paskov and L. I. Pavlov, Appl. Phys. B **54**, 113 (1992).
[36]S. Grabtchak and M. Cocivera, Phys. Rev. B **58**, 4701 (1998).
[37]M. Ichimura, H. Tajiri, Y. Morita, N. Yamada, and A. Usami, Appl. Phys. Lett. **70**, 1745 (1997).
[38]T. Sameshima, H. Hayasaka, and T. Haba, Jpn. J. Appl. Phys. **48**, 021204 (2009).
[39]C. Swiatkowski and M. Kunst, Appl. Phys. A **61**, 623 (1995).
[40]J. Xia and A. Mandelis, Appl. Phys. Lett. **90**, 062119 (2007).
[41]E. Gaubas and A. Kaniava, Rev. Sci. Instrum. **67**, 2339 (1996).
[42]T. S. Horányi, T. Pavelka, and P. Tüttö, Appl. Surf. Sci. **63**, 306 (1993).
[43]A. Sanders and M. Kunst, Solid-State Electron. **34**, 1007 (1991).
[44]J. M. Borrego, R. J. Gutmann, N. Jensen, and O. Paz, Solid-State Electron. **30**, 195 (1987).
[45]J. Chun, A. M. Jones, and J. S. McCloy, J. Appl. Phys. **112**, 023904 (2012).
[46]G. F. Dionne, IEEE Trans. Magn. **39**, 3121 (2003).
[47]A. E. Siegman, *Lasers* (Univ Series Book, Mill Valley, CA, 1986).
[48]K. L. Corum and J. F. Corum, *Tesla's Colorado Springs Receivers* (2003), http://www.teslasociety.com/teslarec.pdf, Electronic document, accessed 7/31/2013.
[49]S. Pipilos, Y. P. Tsividis, J. Fenk, and Y. Papananos, IEEE J. Solid-State Circuits **31**, 1517 (1996).
[50]ARRL, *The Radio Amateur's Handbook* (American Radio Relay League (ARRL), Newington, CT, 1978).

[51]R. Chidambaram, Proc. Indian Acad. Sci. **50**, 63 (1959), http://repository.ias.ac.in/86120/.
[52]D. V. Lang, J. Appl. Phys. **45**, 3023 (1974).
[53]L. Dobaczewski, A. R. Peaker, and K. B. Nielsen, J. Appl. Phys. **96**, 4689 (2004).
[54]C. Hurtes, M. Boulou, A. Mitonneau, and D. Bois, Appl. Phys. Lett. **32**, 821 (1978).
[55]F. L. Walls and J. J. Gagnepain, IEEE Trans. Ultrason. Ferroelectr. Freq. Control **39**, 241 (1992).
[56]P. Raybaut, F. Balembois, F. Druon, and P. Georges, IEEE J. Quantum Electron. **41**, 415 (2005).
[57]R. C. Taber and C. A. Flory, IEEE Trans. Ultrason. Ferroelectr. Freq. Control **42**, 111 (1995).
[58]O. Ishihara, T. Mori, H. Sawano, and M. Nakatani, IEEE Trans. Microwave Theory Tech. **28**, 817 (1980).
[59]T. H. Lee and A. Hajimiri, IEEE J. Solid-State Circuits **35**, 326 (2000).
[60]D. B. Leeson, Proc. IEEE **54**, 329 (1966).